

In the format provided by the authors and unedited.

# Renal clearable catalytic gold nanoclusters for in vivo disease monitoring

Colleen N. Loynachan<sup>1,10</sup>, Ava P. Soleimany<sup>2,3,4,10</sup>, Jaideep S. Dudani<sup>2,5</sup>, Yiyang Lin<sup>1</sup>, Adrian Najer<sup>1</sup>, Ahmet Bekdemir<sup>2,4</sup>, Qu Chen<sup>1</sup>, Sangeeta N. Bhatia<sup>2,4,6,7,8,9\*</sup> and Molly M. Stevens<sup>1\*</sup>

<sup>1</sup>Department of Materials, Department of Bioengineering, and Institute of Biomedical Engineering, Imperial College London, London, UK. <sup>2</sup>Koch Institute for Integrative Cancer Research, Massachusetts Institute of Technology, Cambridge, MA, USA. <sup>3</sup>Harvard Graduate Program in Biophysics, Harvard University, Boston, MA, USA. <sup>4</sup>Harvard-MIT Division of Health Sciences and Technology, Institute for Medical Engineering and Science, Massachusetts Institute of Technology, Cambridge, MA, USA. <sup>5</sup>Department of Biological Engineering, Massachusetts Institute of Technology, Cambridge, MA, USA. <sup>6</sup>Department of Electrical Engineering and Computer Science, Massachusetts Institute of Technology, Cambridge, MA, USA. <sup>7</sup>Department of Medicine, Brigham and Women's Hospital and Harvard Medical School, Boston, MA, USA. <sup>8</sup>Broad Institute of Massachusetts Institute of Technology and Harvard, Cambridge, MA, USA. <sup>9</sup>Howard Hughes Medical Institute, Cambridge, MA, USA. <sup>10</sup>These authors contributed equally: Colleen N. Loynachan, Ava P. Soleimany. \*e-mail: [sbhatia@mit.edu](mailto:sbhatia@mit.edu); [m.stevens@imperial.ac.uk](mailto:m.stevens@imperial.ac.uk)

## **Supplementary Materials and Methods**

### **Solid phase peptide synthesis**

Peptides were synthesized manually on Rink amide resin using standard fluorenyl methoxycarbonyl (Fmoc) chemistry. The Fmoc protecting group was removed from the resin by incubating with piperidine/DMF (20:80) for 2 x 10 min. Fmoc-protected amino acids were activated with 4 molar equivalents of the Fmoc protected amino acids, 3.95 molar equivalents of *N,N,N',N'*-Tetramethyl-*O*-(1*H*-benzotriazol-1-yl)uronium hexafluorophosphate, and 6 molar equivalents of diisopropylethylamine in DMF. The coupling solution was added to the resin and the coupling reaction was allowed to proceed for 3 h. Peptides were cleaved in trifluoroacetic acid/triisopropylsilane/H<sub>2</sub>O (95:2.5:2.5) containing DTT for 4 h. The solvent was removed in vacuum and the peptide was precipitated in cold ether. The crude products were further purified using reversed phase preparative high-performance liquid chromatography (Shimadzu) in an acetonitrile/water gradient under acidic conditions on a Phenomenex C18 Gemini NX column (5 micron pore size, a 110 Å particle size, 150 x 21.2 mm). Molecular weight of peptides was verified using liquid chromatography-mass spectrometry (LC-MS, Agilent Technologies).

### **In vitro gel filtration chromatography (GFC) assays**

AuNC-NAv complexes (10 μM) were first incubated with a recombinant enzyme: MMP9 (Active, Human, Recombinant, PF140, Merck Millipore); MMP7 (Active, Human, Recombinant, *E. coli*, 444270, Merck Millipore); MMP13 (Active, Human, Recombinant, 444287); or thrombin from human plasma (T7009, Sigma, 100 U·mL<sup>-1</sup> in a 0.1% (w/v) bovine serum albumin solution). Enzyme and AuNC-NAv were incubated at 37 °C gently shaking (500 rpm). Incubation times varied (1 – 12 h) and concentration of enzyme was fixed at 50 nM, where the final peptide substrate concentration was maintained at > 1000 molar excess to enzyme concentration.

Three identical glass chromatography columns were packed with Sephacryl S200 high resolution resin (column D: 1 cm, H: 18 cm, resin: GE Healthcare Life Sciences, fractionation range for globular proteins 5– 250 kDa) to separate samples based on size. Columns were thoroughly cleaned between experiments with PBS. In a typical GFC experiment, ca. 200 μL of 10 μM AuNC-PX, AuNC-PX-NAv, and AuNC-PX-NAv + 50 nM enzyme (after incubation) were loaded onto each column in parallel. As soon as the sample was added to the resin bed, 24, 500 μL fractions were collected into individual Eppendorf tubes, while PBS was added to the column reservoir. After fractions were collected, a catalytic activity assay was performed on the samples. For the activity assay, 100 μL of each fraction was added to a 96-well plate,

followed by 100  $\mu\text{L}$  substrate solution (1-Step Ultra TMB ELISA Substrate Solution with 4 M  $\text{H}_2\text{O}_2$ ). The absorbance of the reaction solution at 652 nm was monitored up to 30 min after addition of substrate, corresponding to oxidation of TMB by  $\text{H}_2\text{O}_2$ . The composition of the sample could be determined based on how quickly it eluted from the column as measured by activity. Larger AuNC-NAv complexes eluted within the first 7 mL, and smaller bare AuNCs eluted more slowly and were found in fractions 7 – 12 mL, corroborated by DLS of column fractions. Absorbance at a fixed time point was plotted as a function of eluted volume, where clear peaks in absorbance were associated with either AuNC-NAv complexes or bare AuNCs. For AuNC-NAv complexes incubated with enzymes, the proportion of liberated AuNCs could be measured by calculating the area under the curve corresponding to 7-12 mL eluted volume (fractions corresponding to bare AuNCs) compared to the total area for the entire eluted volume.

### **Fluorescence correlation spectroscopy (FCS)**

FCS is an autocorrelation analysis of temporal fluctuations of fluorescence intensity due to diffusion of fluorescent particles in and out of a small observation volume, useful for monitoring binding or cleavage events by analysing changes in diffusivity over time.

For FCS analysis, AuNC batches were labelled with Oregon Green fluorescent dye (at the free amino group of GSH) and assembled into complexes with the neutravidin core. AuNC-P1 and AuNC-P2 were labelled with 50 molar excess reactive dye (Oregon Green 488 Carboxylic Acid, Succinimidyl Ester, 6-isomer, Thermo Fisher), further called AuNC-PX-OG. Unreacted dye was removed using Zeba Spin Desalting Columns 7K MWCO (Thermo Fisher). AuNC-PX-OG-NAv complexes were assembled following the “AuNC-NAv complex assembly” protocol outlined in the online Methods section, and purified to remove unbound AuNC-PX-OG. AuNC-PX-OG-NAv complexes were further incubated with enzymes, and kinetics of AuNC-NAv complex disassembly via substrate cleavage was monitored over time using FCS.

### **Sample preparation for measuring enzyme cleavage kinetics**

**For MMP9:** 0.33  $\mu\text{L}$  MMP9 stock (Merck PF140 lot#2872521, 0.1  $\text{mg}\cdot\text{mL}^{-1}$  ~ 1500 nM, 57.28 Units/h/ $\mu\text{g}$  P) was added per 10  $\mu\text{L}$  sample stock (20  $\mu\text{M}$ , AuNC), for a final enzyme concentration of 50 nM, with AuNCs in 400 molar excess to MMP9. Since AuNCs bear ca. 20 peptide substrates per particle, there was ca. 8000 molar excess peptide substrates per enzyme. **For thrombin:** 0.58  $\mu\text{L}$  thrombin stock (100  $\text{U}\cdot\text{mL}^{-1}$ , 32  $\mu\text{g}\cdot\text{mL}^{-1}$  ~ 860 nM) was added per 10  $\mu\text{L}$  sample stock (20  $\mu\text{M}$ , AuNC), for a final enzyme concentration of 50 nM, with AuNCs in 400 molar excess to thrombin. All enzyme incubations were performed at 37  $^\circ\text{C}$ , and incubations longer than 3 h were maintained at 37  $^\circ\text{C}$  while shaking (300 rpm). Samples were then diluted in pre-warmed PBS for FCS measurements.

## FCS measurements

In the measurement, labelled particles diffuse through the detection volume, producing a fluctuating fluorescence signal which is subjected to an autocorrelation algorithm yielding an autocorrelation curve,  $G(\tau)$ , which shows the mobility of the particles. The diffusion time of the particles,  $\tau_D$ , can be estimated from the inflection of the decay of the autocorrelation curve.

FCS was performed on a commercial LSM 880 (Carl Zeiss, Jena, Germany) equipped with an incubation chamber. All measurements were performed at 37 °C. An Ar<sup>+</sup> laser was used as excitation source for the 488 nm wavelength. Appropriate filter sets were used to detect the fluorescence signal (LP 505). The laser beam passed through a 40x C-Apochromat water immersion objective with a numeric aperture of 1.2 to focus the beam into the sample droplet. Measurements were performed 200 μm above the ibidi 8-well bottom plate (80826, ibidi, Germany) using a 5 μL droplet of sample for each condition. OregonGreen 488 carboxylic acid in PBS (OG488, O6149, ThermoFisher Scientific, NHS-ester was first deactivated by overnight incubation in PBS at room temperature) was used as a standard to calibrate the beam waist ( $D = 4.1 \times 10^{-6} \text{ cm}^2/\text{s}$  at 25 °C, and when corrected for the higher temperature used:  $D = 5.49 \times 10^{-6} \text{ cm}^2/\text{s}$  at 37 °C).<sup>1</sup> Immediately before the measurement, stocks or incubated samples were diluted 100-fold in pre-warmed PBS and 5 μL was placed into the measuring chamber. The sample was equilibrated and bleached for 5 x 5 s and 25 x 5 s intensity traces were recorded, autocorrelated and analysed for each sample. Autocorrelation curves were created in ZEN software (Carl Zeiss, Jena, Germany) and the curves were exported for further analysis using PyCorrfit program 1.1.1.<sup>2</sup> For all the graphs, data for the 25 curves are given except for the autocorrelation curves, which are always the average curve for the whole measurement (125 s). To calculate the percentage of AuNCs cleaved from the AuNC-NAv complex, stocks of clusters/complexes were first fitted using one component fits ( $G_{1comp}(\tau)$ ) to obtain the diffusion times for the pure components. Second, samples incubated with enzymes were fitted with two component fits ( $G_{2comp}(\tau)$ ) with one component fixed to pure cluster diffusion ( $\tau_1$ ) and the other fixed to pure complex diffusion ( $\tau_2$ ) to yield the fraction of free clusters ( $F_1$ ), which is equivalent to the fraction cleaved. A triplet fraction with a triplet time of 10 μs was included for all the curves.

$$\text{Equation 1: } G_{1comp}(\tau) = \left(1 + \frac{T}{1-T} e^{\frac{-\tau}{\tau_{trip}}}\right) * \frac{1}{N * \left(1 + \frac{\tau}{\tau_D}\right) * \sqrt{1 + \frac{\tau}{SP^2 \tau_D}}}$$

$$\text{Equation 2: } G_{2comp} = \left(1 + \frac{T}{1-T} e^{\frac{-\tau}{\tau_{trip}}}\right) * \frac{1}{N} * \left[ \frac{F_1}{\left(1 + \frac{\tau}{\tau_1}\right) * \sqrt{1 + \frac{\tau}{SP^2 \tau_1}}} + \frac{1 - F_1}{\left(1 + \frac{\tau}{\tau_2}\right) * \sqrt{1 + \frac{\tau}{SP^2 \tau_2}}} \right]$$

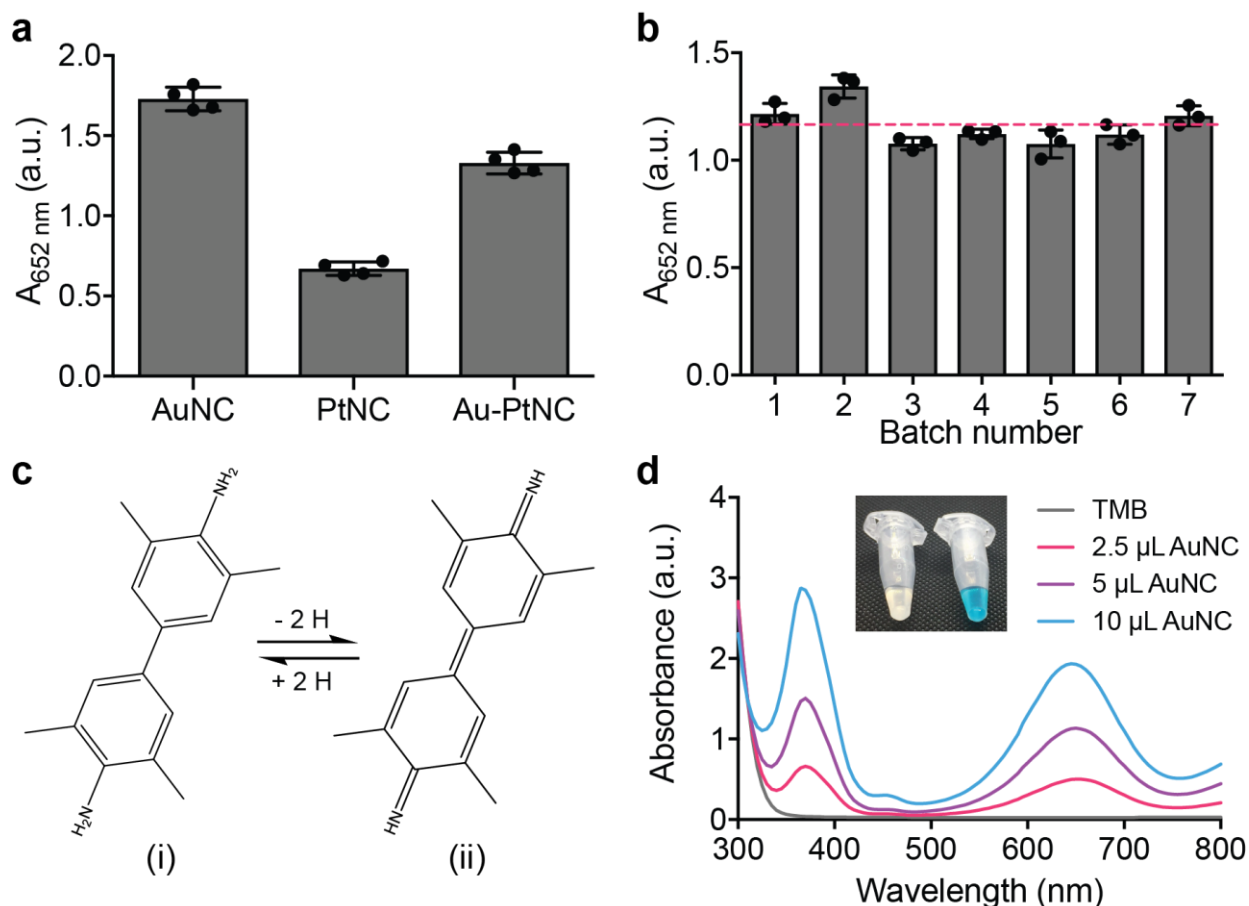
$T$  is the triplet fraction with corresponding triplet time  $\tau_{trip}$ ,  $N$  is the effective number of diffusing species in the confocal volume ( $N = n_1 + n_2$ ),  $\tau_D$  is the diffusion time ( $\tau_1, \tau_2$  diffusion times of corresponding fractions),  $F_1$  fraction of component with diffusion time  $\tau_1$ , and  $SP$  is the structural parameter describing the ratio of height to width of the confocal volume (fixed to 5). The following equation relates the x-y dimension of the confocal volume ( $\omega_{xy}^2$ ), which was calibrated by a standard measurement of OG488 in PBS, to the diffusion coefficient ( $D$ ), which was calculated for each sample using the obtained diffusion time ( $\tau_D$ ):

$$\text{Equation 3: } D = \frac{\omega_{xy}^2}{4\tau_D}$$

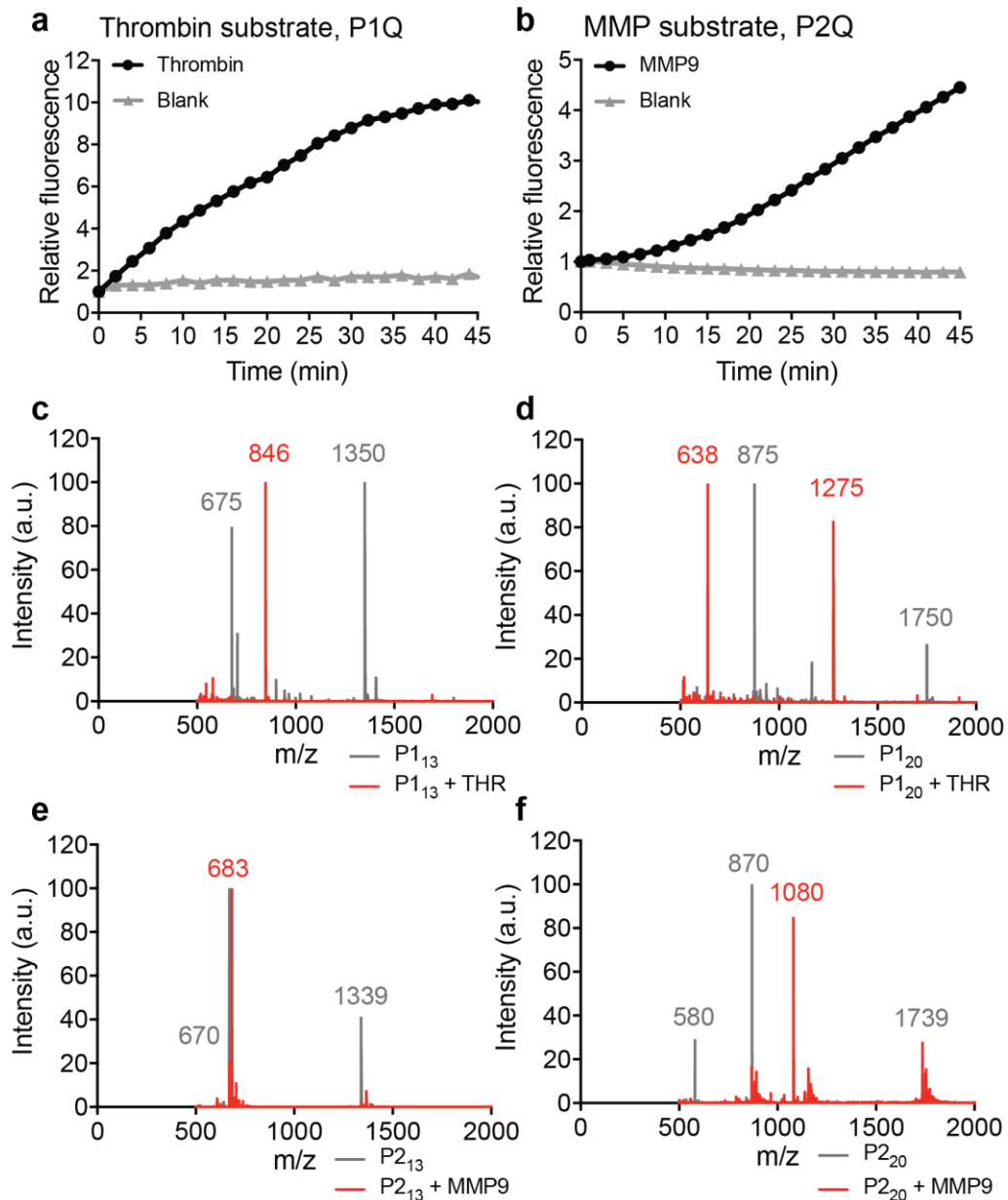
Stokes-Einstein equation was used to calculate hydrodynamic diameter via the obtained diffusion coefficients. For the AuNC-P2<sub>13</sub>-NAv complex, the percentage of cleaved AuNCs with time was linear over the first 500 min. of MMP9 incubation, whereas for AuNC-P2<sub>20</sub>-NAv the percentage cleaved was linear over just the first 16 min. of enzyme incubation. The linear regions were analysed by linear regression, and the rates of cleavage were calculated.

### ***In vitro* cleavage assays with quenched substrates**

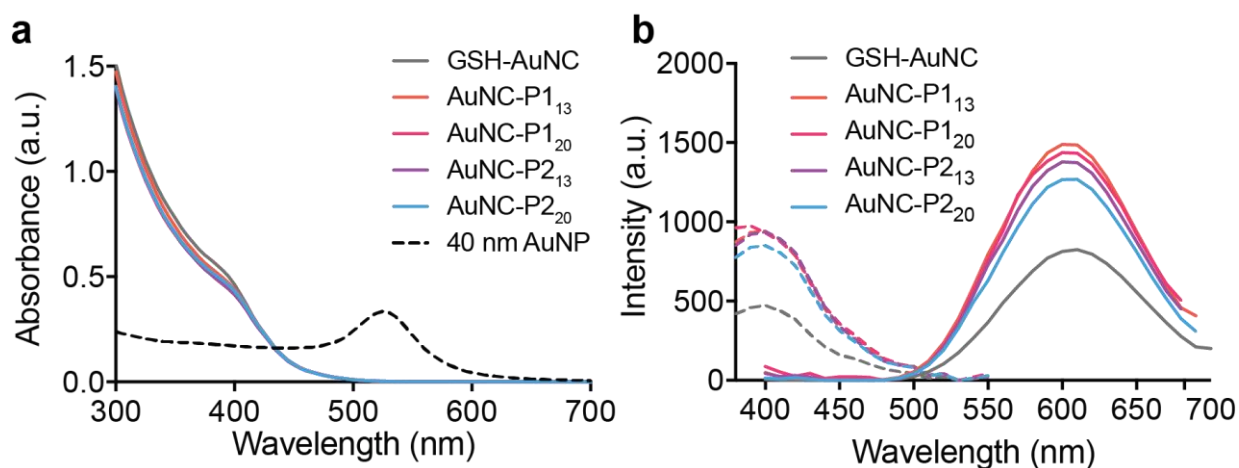
P1Q (1  $\mu$ M by peptide) was incubated with recombinant mouse thrombin (12.5 nM working concentration; Haematologic Technologies) in a 384-well plate at 37°C in PBS-BSA (0.1% w/v). P2Q (1  $\mu$ M by peptide) was incubated with recombinant human MMP-9 (100 nM working concentration; Enzo Life Sciences) in activity buffer (50 mM Tris, 150 mM NaCl, 5 mM CaCl<sub>2</sub>, 1  $\mu$ M ZnCl<sub>2</sub>) containing 0.1 wt% BSA. Fluorescence dequenching was monitored at 37 °C using a Tecan Infinite 200pro microplate reader (Tecan).



**Supplementary Figure 1.** Synthesis of peptide-templated nanoclusters. (a) Catalytic activity of glutathione-templated nanoclusters synthesized with varying core metals: gold, platinum, and gold-platinum bimetallic hybrid. AuNCs exhibited the highest activity followed by Au-Pt with intermediate activity, and PtNCs showed the lowest activity of the tested metals when synthesized with a fixed GSH:[Metal] of 1.5 (mean  $\pm$  s.d.,  $n = 4$  independent experiments). (b) AuNC synthesis showed high reproducibility in terms of catalytic activity with a coefficient of variation between 7 independently synthesized batches of 8.5% (mean  $\pm$  s.d.,  $n = 3$  independent experiments). The red line indicates the average catalytic activity measured as absorbance at 652 nm corresponding to the oxidation of TMB across 7 AuNC batches. (c) Structure of 3,3',5,5'-tetramethylbenzidine (TMB) (i), and oxidized TMB (TMB diimine) (ii). (d) Representative UV/vis spectra showing increase in absorbance correlated to oxidation of TMB in presence of varying concentrations of AuNCs, where the experiment was repeated independently 3 times with similar results. An increase in absorbance at both 370 nm and 652 nm was observed for increasing concentration of nanocatalyst with fixed concentrations of TMB and  $\text{H}_2\text{O}_2$  substrates. Inset shows photo of substrate alone (left) and substrate with AuNCs with blue colour development (right).

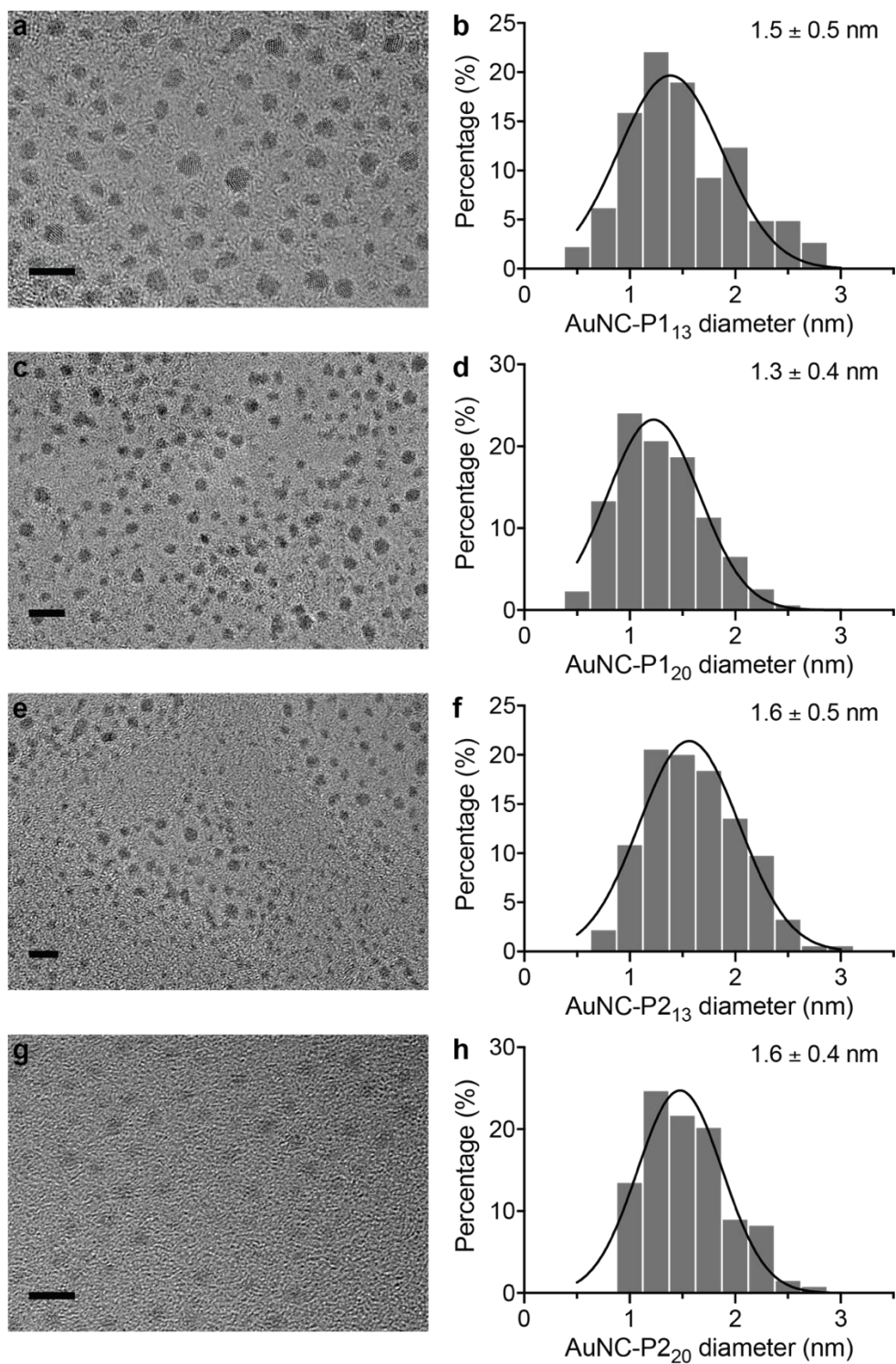


**Supplementary Figure 2.** Proteolytic cleavage of peptide substrates. (a) and (b) Fluorescently quenched thrombin- or MMP-responsive (a and b, respectively) peptides were incubated with target enzyme (human thrombin or human MMP9, respectively). Proteolytic cleavage released the quencher, and fluorescence was measured to monitor cleavage kinetics (mean,  $n = 2$  independent measurements). (c) and (d) Liquid chromatography-mass spectrometry (LC-MS) chromatograms of thrombin-responsive P1<sub>13</sub> and P1<sub>20</sub> peptides (c and d, respectively) following 12 h incubation with recombinant thrombin, where the experiments were repeated independently 3 times with similar results. (e) and (f) LC-MS chromatograms of MMP-responsive P2<sub>13</sub> and P2<sub>20</sub> peptides (e and f, respectively) following 12 h incubation with recombinant MMP9, where the experiments were repeated independently 3 times with similar results.

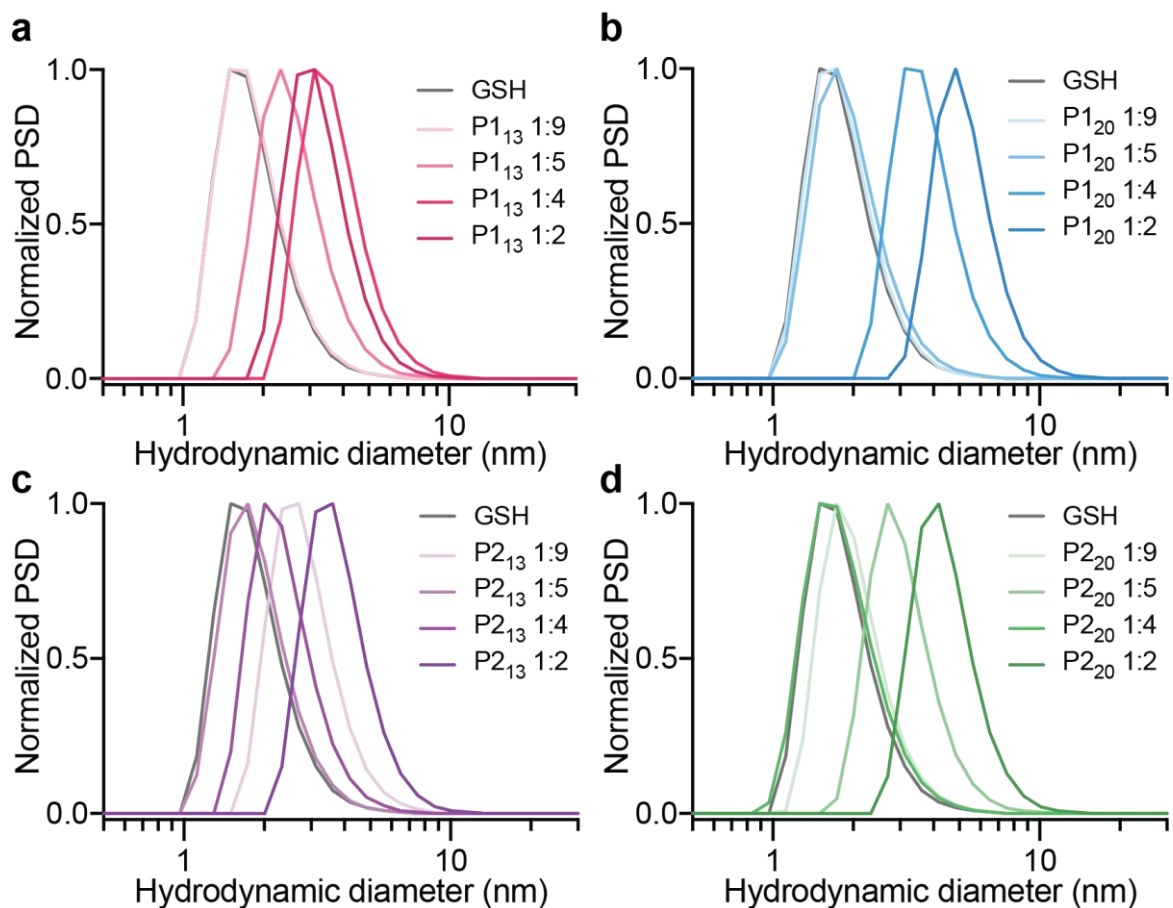


**Supplementary Figure 3.** Characterization of optical properties of AuNCs. (a) UV/vis absorption spectrum of peptide-templated AuNC batches compared to 40 nm gold nanoparticles (AuNPs). AuNCs did not exhibit surface plasmon resonance peak at 520 nm characteristic of larger AuNPs. (b) Fluorescence excitation (Em: 600 nm, dotted line) and emission (Ex: 400 nm, solid line) spectrum. Experiments were repeated independently 3 times with similar results.

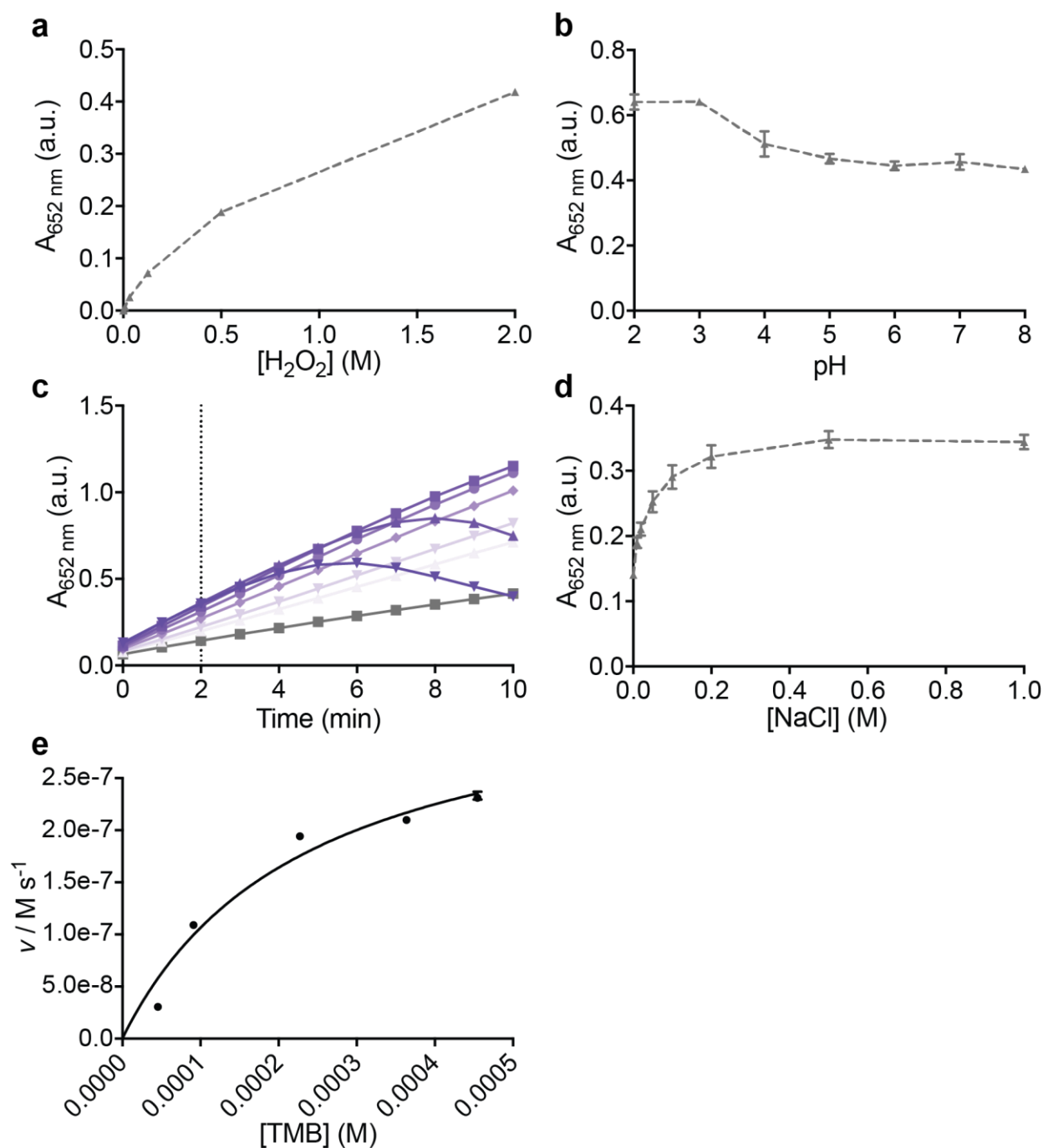




**Supplementary Figure 4.** Representative TEM images of AuNCs synthesized with different peptide sequences and corresponding particle size analysis. (a, b) AuNC-P1<sub>13</sub>, (c, d) AuNC-P1<sub>20</sub>, (e, f) AuNC-P2<sub>13</sub>, (g, h) AuNC-P2<sub>20</sub>. Scale bars, 5 nm; legends in b ( $n = 227$ ), d ( $n = 354$ ), f ( $n = 185$ ), and h ( $n = 134$ ) show mean diameter  $\pm$  s.d.

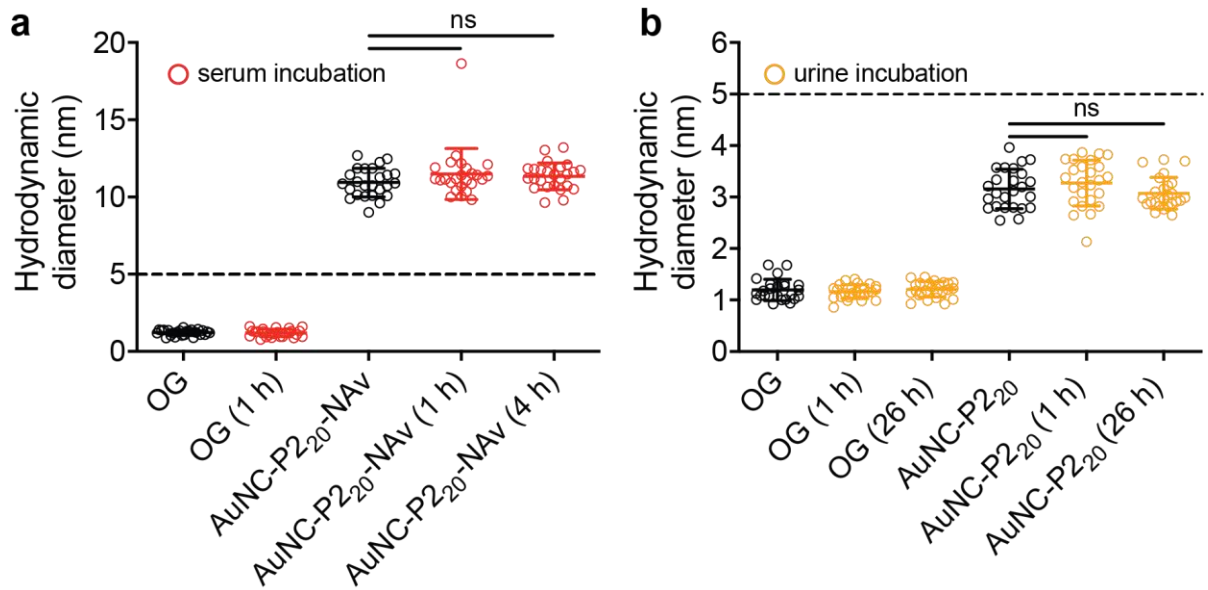


**Supplementary Figure 5.** Number particle size distribution (PSD) measured by dynamic light scattering (DLS) of AuNCs synthesized with different peptide sequences (a) P1<sub>13</sub>, (b) P1<sub>20</sub>, (c) P2<sub>13</sub>, (d) P2<sub>20</sub>. Increasing intensity of coloured line corresponds to increasing concentration of protease-cleavable peptide sequence in synthesis. Ratios in legends correspond to the PX:glutathione ratio (1:9, 1:5, 1:4, 1:2) used in synthesis. All particles were synthesized with a fixed total peptide concentration and DLS experiments were repeated independently 3 times with similar results.

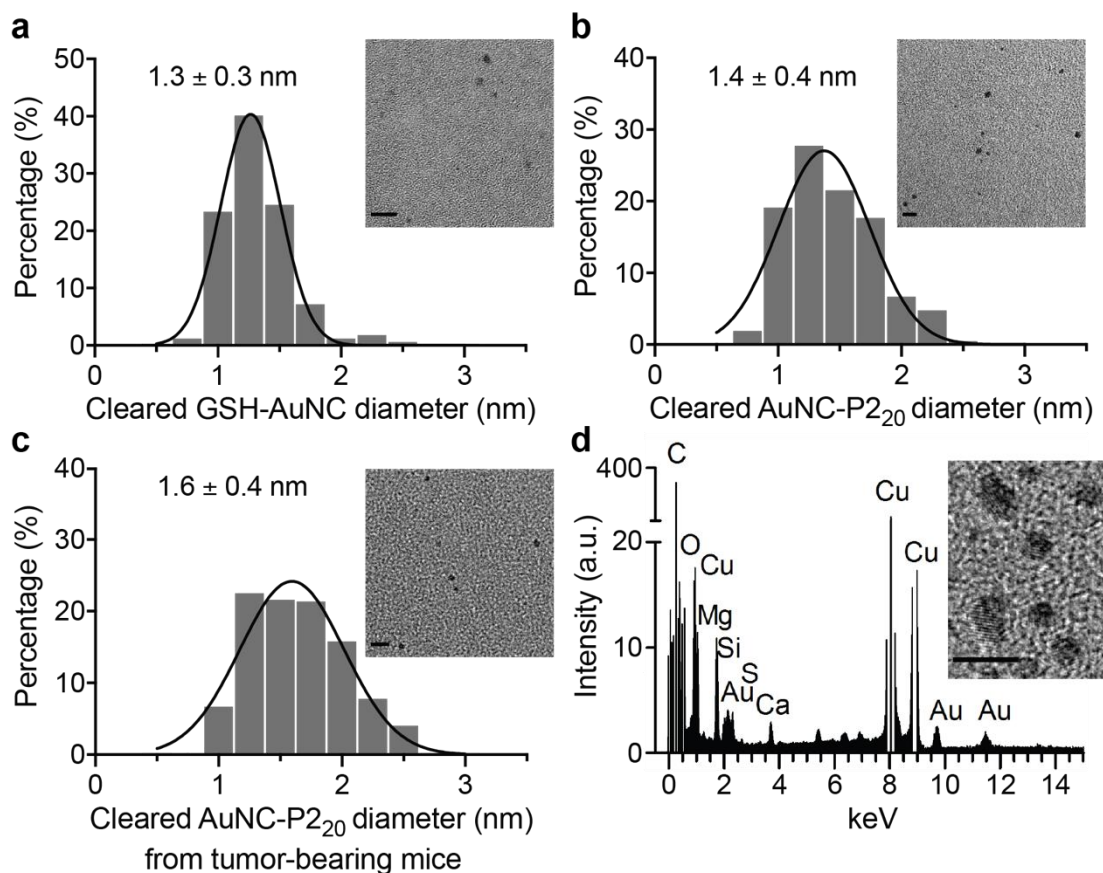


**Supplementary Figure 6.** Characterization and optimization of catalytic activity assay conditions. (a) Catalytic activity of GSH-AuNCs as a function of hydrogen peroxide concentration (mean  $\pm$  s.d.,  $n = 3$  independent experiments). Activity was measured by the absorbance at 652 nm corresponding to the oxidation of TMB by H<sub>2</sub>O<sub>2</sub>. Colorimetric signal increased with increasing concentration of hydrogen peroxide in assay buffer. (b) Catalytic activity of GSH-AuNCs as a function of pH (mean  $\pm$  s.d.,  $n = 3$  independent experiments). (c) Kinetic measurement of catalytic activity with varying sodium chloride concentration (gray: no salt; increasing colour intensity: 0.01, 0.02, 0.05, 0.1, 0.2, 0.5, 1 M NaCl), where precipitation of substrate occurred at high [NaCl]. Experiment was repeated independently 3 times with similar results. (d) Catalytic activity with varying [NaCl] after 2 min development (dotted line in Supplementary Fig. 6c, mean  $\pm$  s.d.,  $n = 3$  independent experiments). PBS spiked with ca. 2.5 M H<sub>2</sub>O<sub>2</sub> was selected as the assay reaction buffer due to its acidic pH and optimal salt concentration. (e) Steady-state kinetic assays of GSH-AuNCs as catalysts for the oxidation of

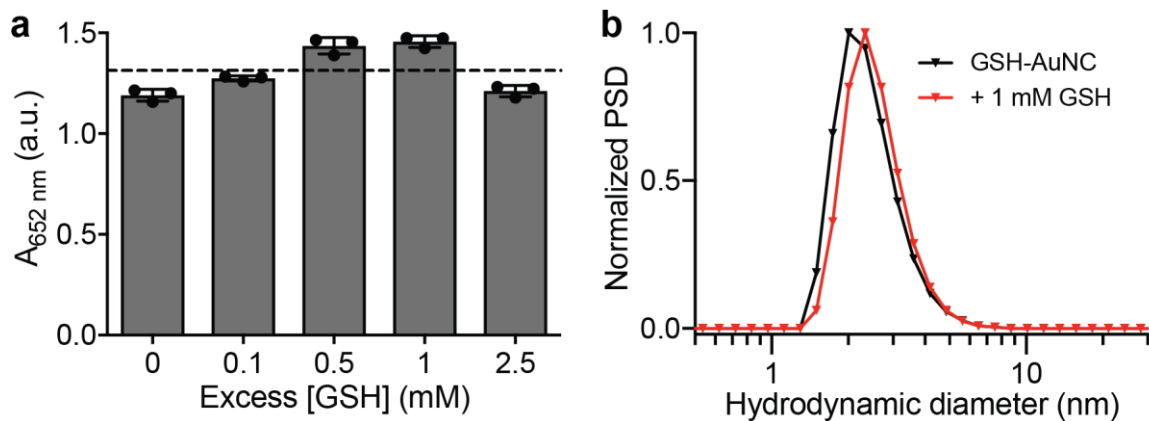
TMB by  $\text{H}_2\text{O}_2$  (mean  $\pm$  s.d.,  $n = 3$  independent experiments). The initial reaction velocity ( $v$ ) was measured in 25 mM sodium acetate buffer pH 4.0 with  $1.8 \times 10^{-6}$  M AuNCs at room temperature over 150 seconds. Plot of  $v$  against TMB concentration, in which  $\text{H}_2\text{O}_2$  was fixed at 2.3 M.



**Supplementary Figure 7.** Hydrodynamic diameters calculated from FCS autocorrelation curves showing sizes of Oregon Green (OG) fluorescent dye, AuNC-NAV complexes, and AuNCs after incubation in PBS (black) or physiological environments (red or yellow). (a) AuNC-P2<sub>20</sub>-NAV complex incubated in PBS (black) or 10% v/v fetal bovine serum (FBS, red) for 1 h and 4 h (one-way ANOVA with Dunnett's multiple comparison, <sup>ns</sup>*P* = 0.187 for 1 h, <sup>ns</sup>*P* = 0.382 for 4 h). (b) AuNC-P2<sub>20</sub> incubated in PBS (black) or undiluted synthetic urine (yellow) for 1 h and 26 h (one-way ANOVA with Dunnett's multiple comparison, <sup>ns</sup>*P* = 0.470 for 1 h, <sup>ns</sup>*P* = 0.657 for 26 h). Dashed line represents renal filtration size cut-off of ca. 5 nm. Individual sample measurements are represented as open circles with overlaid mean and standard deviation (*n* = 25 independent measurements).

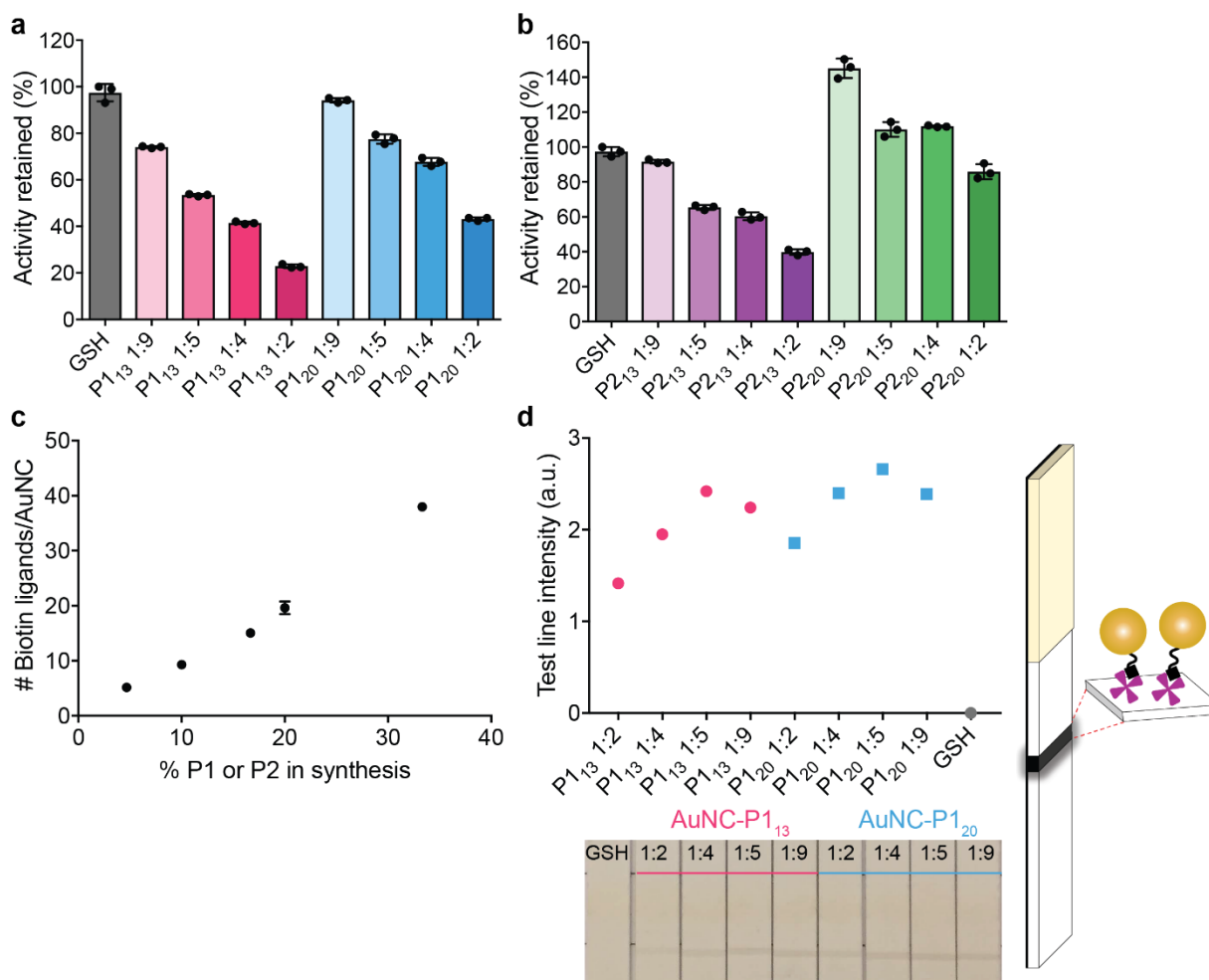


**Supplementary Figure 8.** Characterization of AuNCs in urine after kidney filtration. Histogram showing results of size analysis from TEM images of (a) GSH-AuNCs (legend shows mean diameter  $\pm$  s.d.,  $n = 167$  particles) and (b) AuNC-P2<sub>20</sub> ( $n = 209$  particles) in mouse urine that was collected 1 h p.i. with AuNC samples. (c) AuNCs in mouse urine 1 h p.i. of MMP9-responsive AuNC-P2<sub>20</sub>-NAV complexes in tumour-bearing mice, indicating successful cleavage and renal elimination of liberated AuNCs in tumour model ( $n = 449$  particles). Solid line represents Gaussian fit of size distribution. Inset shows representative TEM images used for size analysis for each particle batch (scale = 5 nm). AuNC samples in urine were desalted and purified through centrifugal ultrafiltration prior to imaging. (d) Energy Dispersive X-ray (EDS) point spectra analysis of the elemental composition of randomly selected areas across TEM grids containing cleared GSH-AuNCs in urine, where the experiment was repeated independently 3 times with similar results. EDS spectrum confirms the presence of gold and other elements that may be excreted by the kidneys, including calcium and magnesium, in addition to copper, carbon, and silicon signal from the TEM grid. Inset shows representative TEM image of grid area used for EDS analysis showing lattice fringes on renally cleared AuNCs (scale = 5 nm).



**Supplementary Figure 9.** Stability of AuNCs in presence of physiological glutathione concentrations. (a) Catalytic activity of GSH-AuNCs incubated with excess glutathione up to 2.5 mM for 1 h at 37 °C. The dashed line indicates the average catalytic activity measured as absorbance at 652 nm corresponding to the oxidation of TMB across all samples analysed (mean  $\pm$  s.d.,  $n = 3$  independent experiments). (b) Number particle size distribution (PSD) measured by DLS of GSH-AuNCs in PBS (black) and GSH-AuNCs incubated in the presence of 1 mM glutathione for 1 h at 37 °C (red), where the DLS experiment was repeated independently 3 times with similar results.

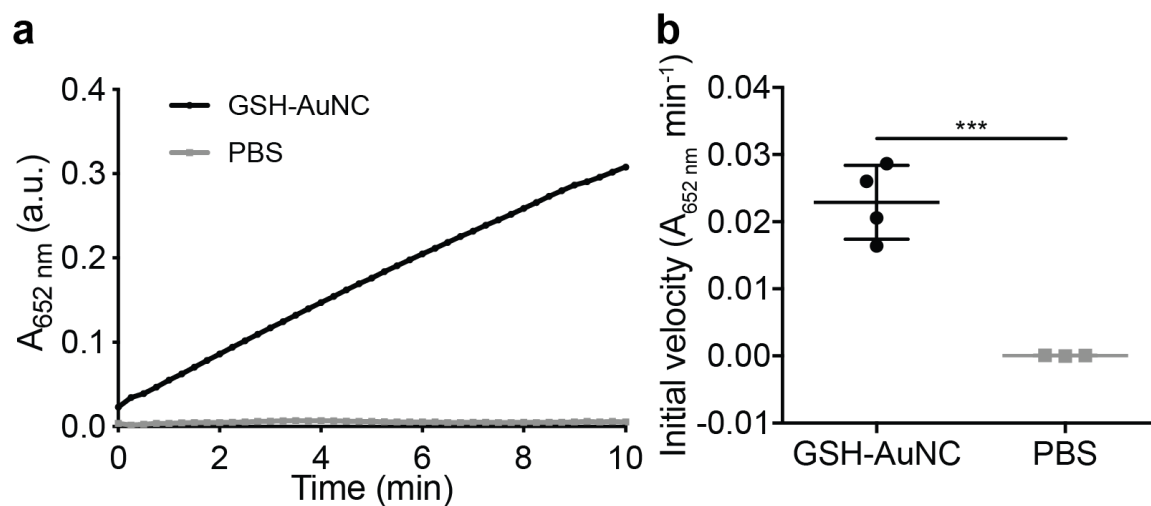




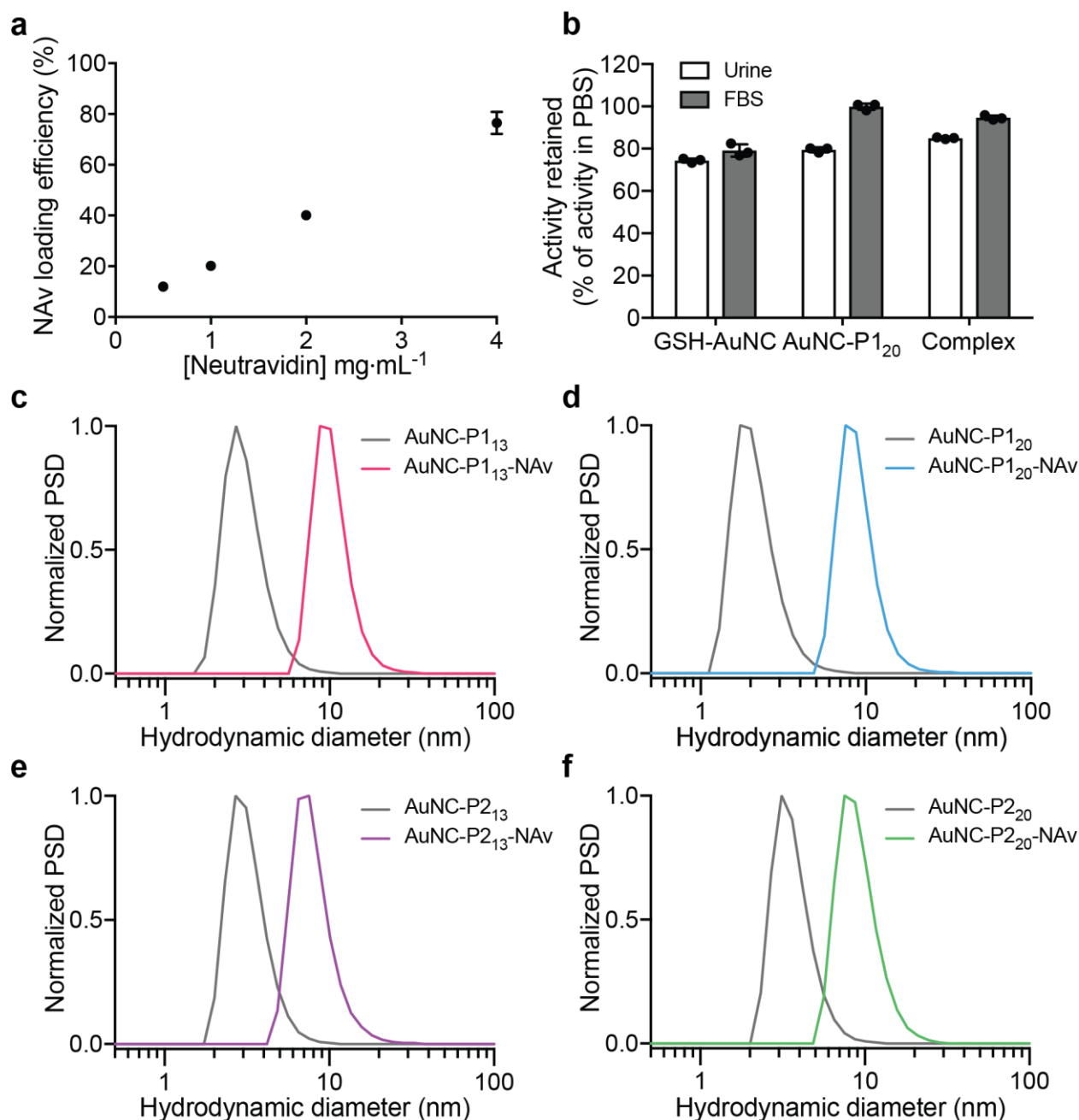
**Supplementary Figure 10.** Characterization of AuNCs functionalized with protease-responsive peptides. (a, b) Catalytic activity of AuNCs synthesized with varying protease-cleavable peptide sequences (P1<sub>13</sub>, P1<sub>20</sub>, P2<sub>13</sub>, P2<sub>20</sub>) and varying ratios of protease-cleavable peptide sequence to glutathione (PX:glutathione in ratios 1:9, 1:5, 1:4, 1:2), where activity is normalized to activity of AuNCs synthesized in the absence of P1<sub>13</sub> or P1<sub>20</sub>, P2<sub>13</sub> or P2<sub>20</sub> (glutathione only, GSH-AuNCs). Activity decreased with increasing amount of P1 or P2 incorporated onto the AuNC surface. This change could be ascribed to the bulkier peptides replacing GSH in the synthesis, which may block access to the AuNC surface, decreasing surface area available for interaction with substrate molecules and subsequent catalytic reactions. The biotinylated protease substrate is required to form the AuNC-NAv complex; however, increasing the number of P1 or P2 peptides per AuNC resulted in a decrease in activity, thus requiring a careful balance of synthesis parameters. The differences in catalytic activity with varying peptide sequence may be attributed to variations in peptide hydrophobicity, charge, and molecular weight affecting accessibility and affinity of substrate molecules for the catalytic surface. (c) Quantification of biotin ligands per AuNC when ratio of peptide sequence (P1<sub>13</sub> or P2<sub>13</sub> or P2<sub>20</sub>) to glutathione was varied in the synthesis. Amount of biotin in supernatant of AuNC synthesis after purification was measured using 4'-hydroxyazobenzene-2-carboxylic acid (HABA)-avidin reagents, and biotin concentration on the particles was extrapolated using the starting concentration of biotin in synthesis and estimated concentration of AuNCs. (d) The functional performance of the AuNC batches containing different ratios of the protease-cleavable substrates on the surface was tested using a paper-based assay (schematic on right). The assay used a streptavidin test line to measure the ability of the AuNC to effectively bind to avidin and a subsequent catalytic development step to probe the activity of the particles. We found that there was an optimal ratio of protease substrate incorporated in the



synthesis which led to efficient capping of the gold core with biotinylated protease-cleavable ligands, while retaining activity to preserve diagnostic sensitivity (1:5 ratio for thrombin substrates (P1) and a 1:4 ratio for MMP substrates (P2), which was taken forward in synthesis of particles in the following figures). The optimal substrate incorporation for efficient synthesis corresponded to *ca.* 15 – 20 biotinylated protease substrates per AuNC, where *ca.* 20% of the ligands were protease-cleavable peptides and the remaining capping ligands were glutathione molecules. Test line intensity quantified in ImageJ corresponded to AuNC-P1<sub>13 or 20</sub> binding to polystreptavidin test line, where the experiment was repeated independently 3 times with similar results. AuNCs bound at the test line catalyze the oxidation of CN/DAB (4-chloro-1-naphthol/3,3'-diaminobenzidine tetrahydrochloride) substrate in the presence of hydrogen peroxide producing an insoluble black product. All error bars indicate mean  $\pm$  s.d.,  $n = 3$  independent experiments.

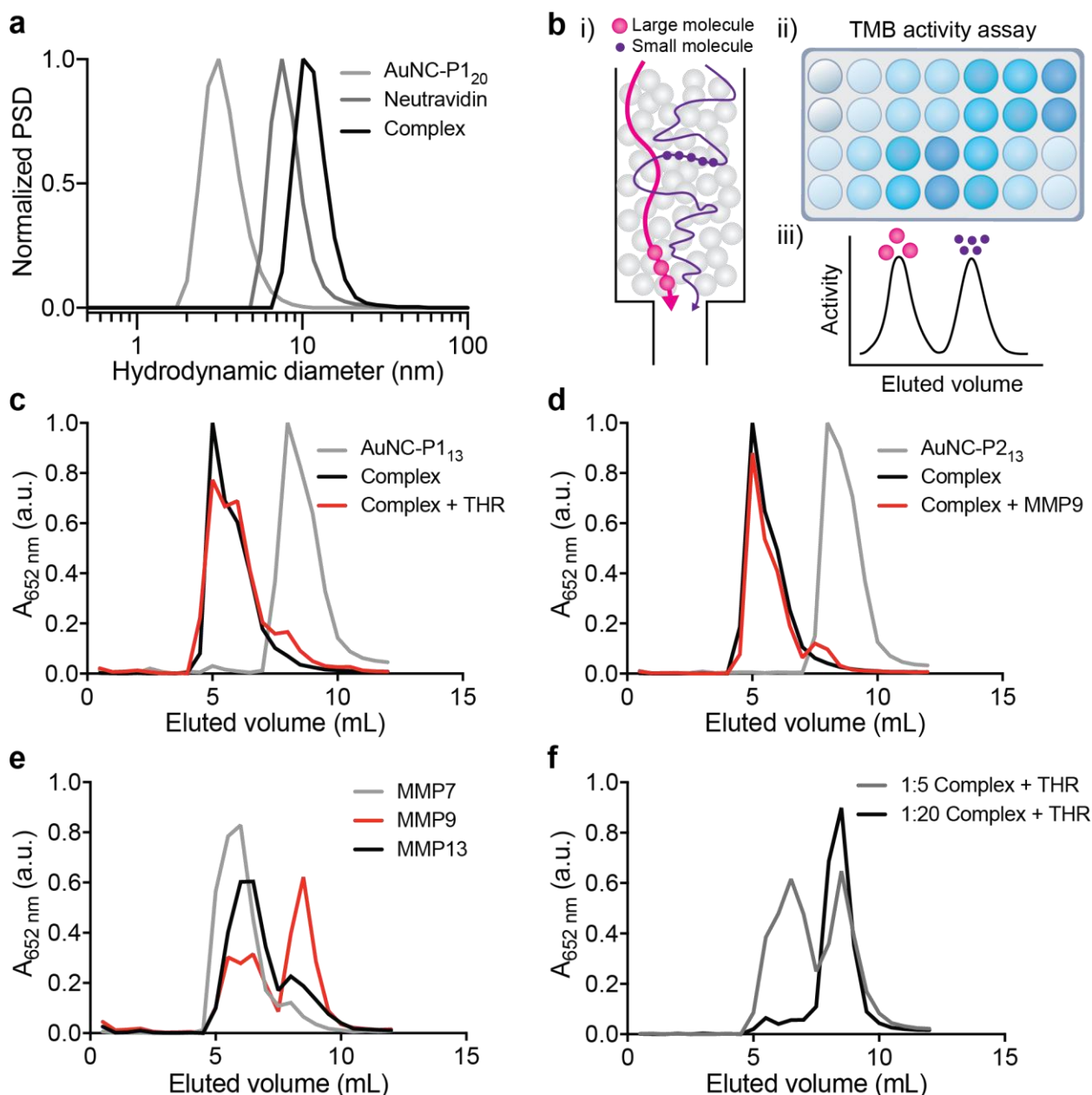


**Supplementary Figure 11.** Assessment of endogenous peroxidase activity in mouse urine. (a) Representative kinetic measurement of catalytic activity in urine samples of mice injected with GSH-AuNCs or PBS. (b) Quantification of initial velocity of catalytic activity from (a), as measured by the rate of change of  $A_{652 \text{ nm}}$  over the first 10 minutes of the reaction (mean  $\pm$  s.d.,  $n = 3$  mice for PBS injection and  $n = 4$  mice for GSH-AuNC injection, two-tailed Student's  $t$ -test, \*\*\* $P = 0.0009$ ).



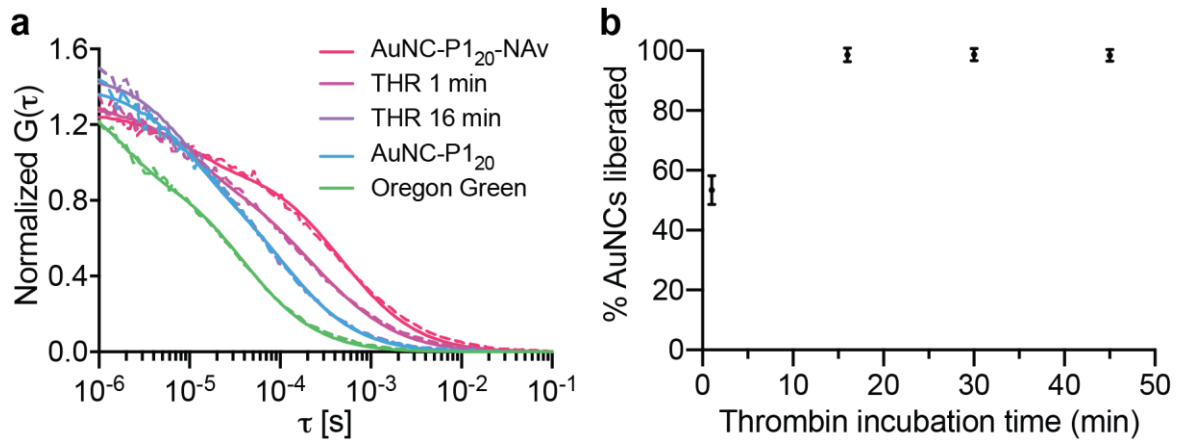
**Supplementary Figure 12.** Synthesis efficiency, serum stability, and size characterization of AuNC-NAv complexes. (a) Quantification of efficiency of binding of biotinylated AuNCs to neutravidin protein for varying neutravidin concentrations, where 4 mg·mL<sup>-1</sup> represents a 1.2 molar excess of AuNCs to neutravidin carrier protein, and 0.5 mg·mL<sup>-1</sup> represents a 9.6 molar excess of AuNCs to neutravidin (mean  $\pm$  s.d.,  $n = 3$  independent experiments). Loading efficiency was measured by calculating the difference in catalytic activity of AuNC-NAv complex before and after ultrafiltration purification to remove unbound AuNCs. Incubation with higher concentrations of neutravidin increased the efficiency of complex formation by up to 70%. While theoretically four biotins should be able to simultaneously bind one neutravidin carrier, it was not possible to load more than two AuNCs on a neutravidin core, even with a large excess of AuNCs (10 molar excess of AuNCs to protein). This could be in part due to steric hindrance. Each AuNC has ca. 20 biotin ligands, so it is also possible that one AuNC could exhibit multivalent binding to the neutravidin core. (b) Catalytic activity of AuNCs and AuNC-NAv complex after incubation in urine (undiluted) or fetal bovine serum (undiluted FBS) environments for 1 h. Activity was normalized to activity of sample in PBS (mean  $\pm$  s.d.,  $n = 3$

independent experiments). (c-f) Number particle size distribution of hydrodynamic diameter measured by DLS for AuNC-P1<sub>13</sub>, -P1<sub>20</sub>, -P2<sub>13</sub>, -P2<sub>20</sub> and corresponding AuNC-NA<sub>v</sub> complexes prepared with each particle batch after purification. DLS experiments were repeated independently 3 times with similar results.

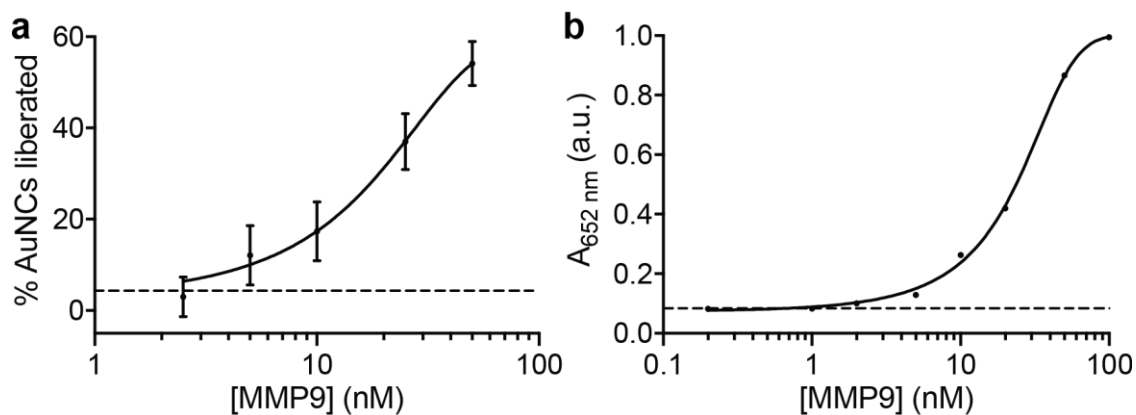


**Supplementary Figure 13.** Gel filtration chromatography (GFC) analysis for monitoring AuNC-NAV complex dissociation. (a) Number distribution of the hydrodynamic diameter of AuNC-P1<sub>20</sub>, neutravidin protein, and AuNC-NAV complex (Complex) measured by DLS. (b) Schematic of *in vitro* assay to monitor size of AuNC-NAV complex in response to recombinant protease activity. (i) Gel filtration chromatography was used to separate molecules based on size (free AuNCs are smaller than AuNC-NAV complex). (ii) Catalytic activity assay was performed on collected column fractions. (iii) Activity of column fractions was plotted against eluted volume and area under the curve was used to determine the ratio of free AuNCs to complex. (c) AuNC-P1<sub>13</sub>, AuNC-P1<sub>13</sub>-NAV complex (Complex), and 10  $\mu$ M AuNC-P1<sub>13</sub>-NAV complex incubated with 50 nM thrombin for 12 h at 37  $^{\circ}$ C (Complex + THR). (d) AuNC-P2<sub>13</sub>, AuNC-P2<sub>13</sub>-NAV complex (Complex), and 10  $\mu$ M AuNC-P2<sub>13</sub>-NAV complex incubated with 50 nM MMP9 for 12 h at 37  $^{\circ}$ C (Complex + MMP9). (e) AuNC-P2<sub>20</sub>-NAV complex incubated with 50 nM MMP7, MMP9, or MMP13 for 12 h at 37  $^{\circ}$ C. The MMP-responsive nanosensor was cleaved more robustly by MMP9 (gelatinase) than by MMP7 (matrilysin) or MMP13 (collagenase). (f) Activity of GFC column fractions for AuNC-NAV complexes prepared with different P1<sub>20</sub> loadings (P1<sub>20</sub>:GSH 1:5 or 1:20), where 1:5 case has ca. 20 biotin ligands per

AuNC and 1:20 case has *ca.* 5 biotin ligands per AuNC, for 1 h incubation with 50 nM thrombin at 37 °C. We hypothesized that by reducing the number of biotin ligands on the AuNC surface, we would have a higher probability of an enzyme cleavage event specifically liberating an AuNC from the complex, rather than cleaving off peptides that are not actively tethering the AuNC to the core. Indeed, we did see this effect, where for AuNCs with only 5 biotin ligands per cluster we observed *ca.* 40% more cleavage than for AuNCs presenting 20 biotin ligands per cluster for 1 h incubation with 50 nM thrombin. However, forming the AuNC-NAv complex is over twice as efficient when the AuNCs present 20 biotin ligands per AuNC, so we maintained this loading for the current study. All DLS and GFC experiments were repeated independently 3 times with similar results.

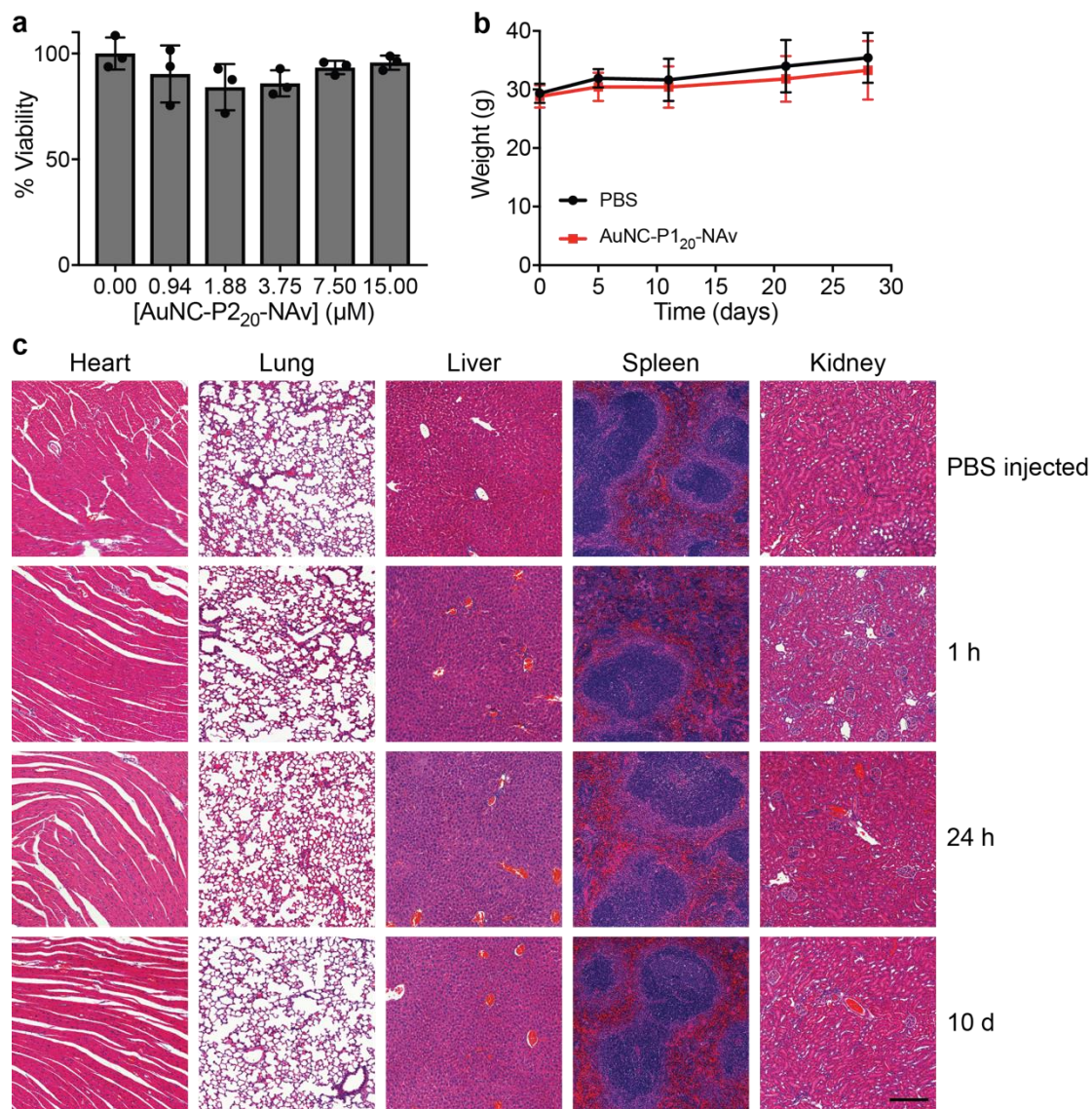


**Supplementary Figure 14.** Cleavage kinetics of thrombin-responsive nanosensor. (a) Average autocorrelation curves from FCS measurements ( $n = 25$  independent measurements) showing AuNC-P1<sub>20</sub>-NAv complex in the presence of thrombin over time compared to free labelled AuNCs and Oregon Green dye (dashed lines: experimental; solid lines: fits). A clear shift to faster diffusion times was observed for longer enzyme incubation times where the complex incubated with thrombin for 16 min (purple) overlaps with the AuNC-P1<sub>20</sub> curve (blue), indicating complete cleavage of AuNCs from the complex in this timeframe. (b) Plot of fraction of AuNCs liberated (see FCS in Supplementary Methods) from AuNC-P1<sub>20</sub>-NAv complex incubated with thrombin (50 nM) up to 45 min. (mean  $\pm$  s.d.,  $n = 25$  independent measurements).

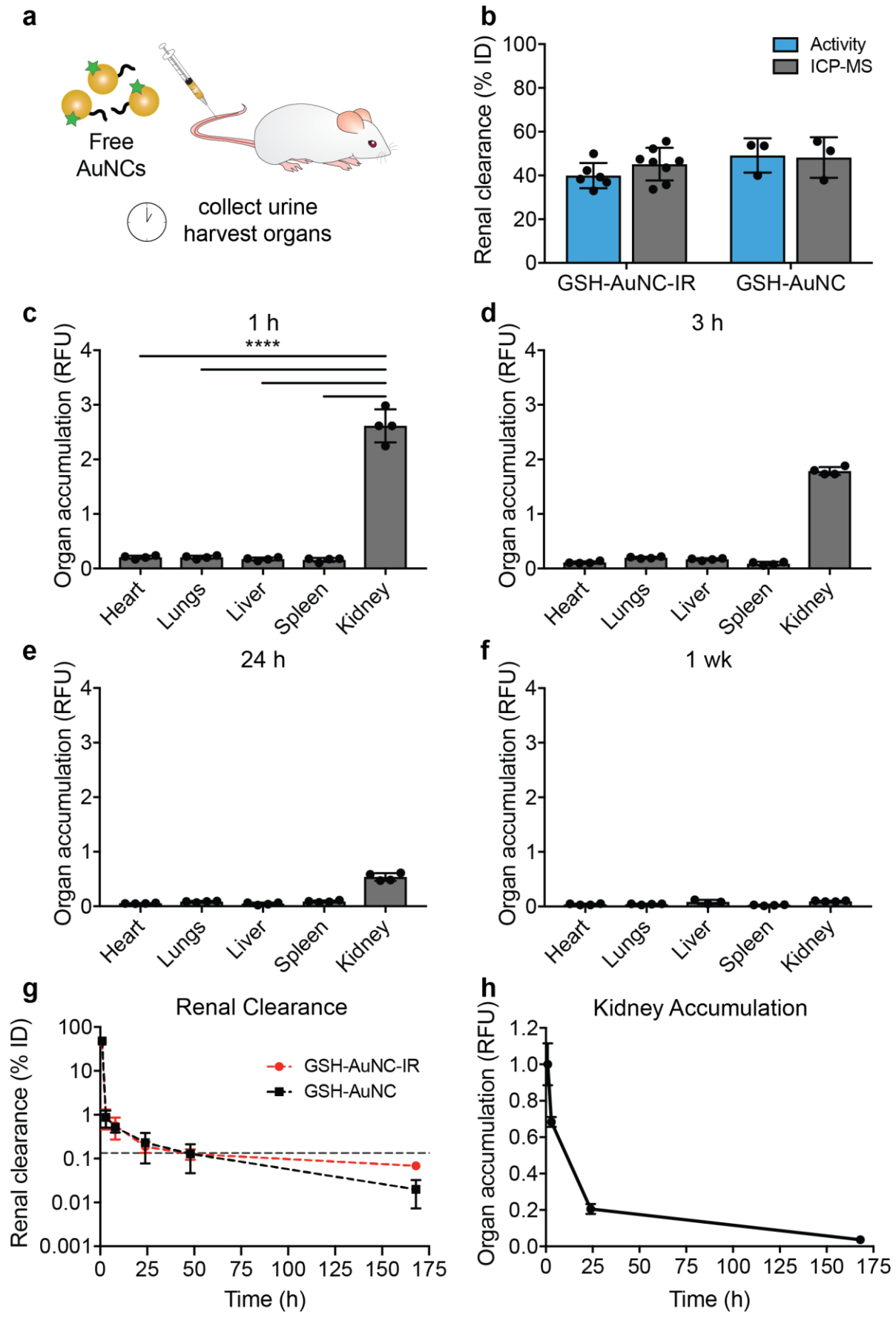


**Supplementary Figure 15.** Probing MMP9 *in vitro* limit of detection. (a) Plot of fraction of AuNCs liberated (see FCS in Supplementary Methods) from AuNC-P2<sub>20</sub>-NAv (15  $\mu$ M) incubated with varying concentrations of MMP9 (2.5 – 50 nM) for 1 h to mimic *in vivo* experimental time frame (mean  $\pm$  s.d.,  $n = 25$  independent measurements). To assemble the complexes for FCS analysis, the AuNC-P2<sub>20</sub> were first labelled with Oregon Green (OG<sub>488 nm</sub>) dye prior to forming a complex with neutravidin. Dashed line represents mean of background signal (samples spiked with PBS instead of MMP9). (b) Plot of absorbance (proportional to catalytic activity of AuNCs) of filtrate containing liberated AuNCs after incubation of AuNC-P2<sub>20</sub>-NAv (15  $\mu$ M) with varying concentrations of MMP9 (0.2 – 100 nM) for 1 h to mimic *in vivo* experimental time frame (mean  $\pm$  s.d.,  $n = 3$  independent experiments) and separated using 50 kDa cut-off centrifugal filter (pore size *ca.* 5 nm). Dashed line represents the detection cut-off calculated as 3 standard deviations above the mean of the background signal (samples spiked with PBS instead of MMP9).

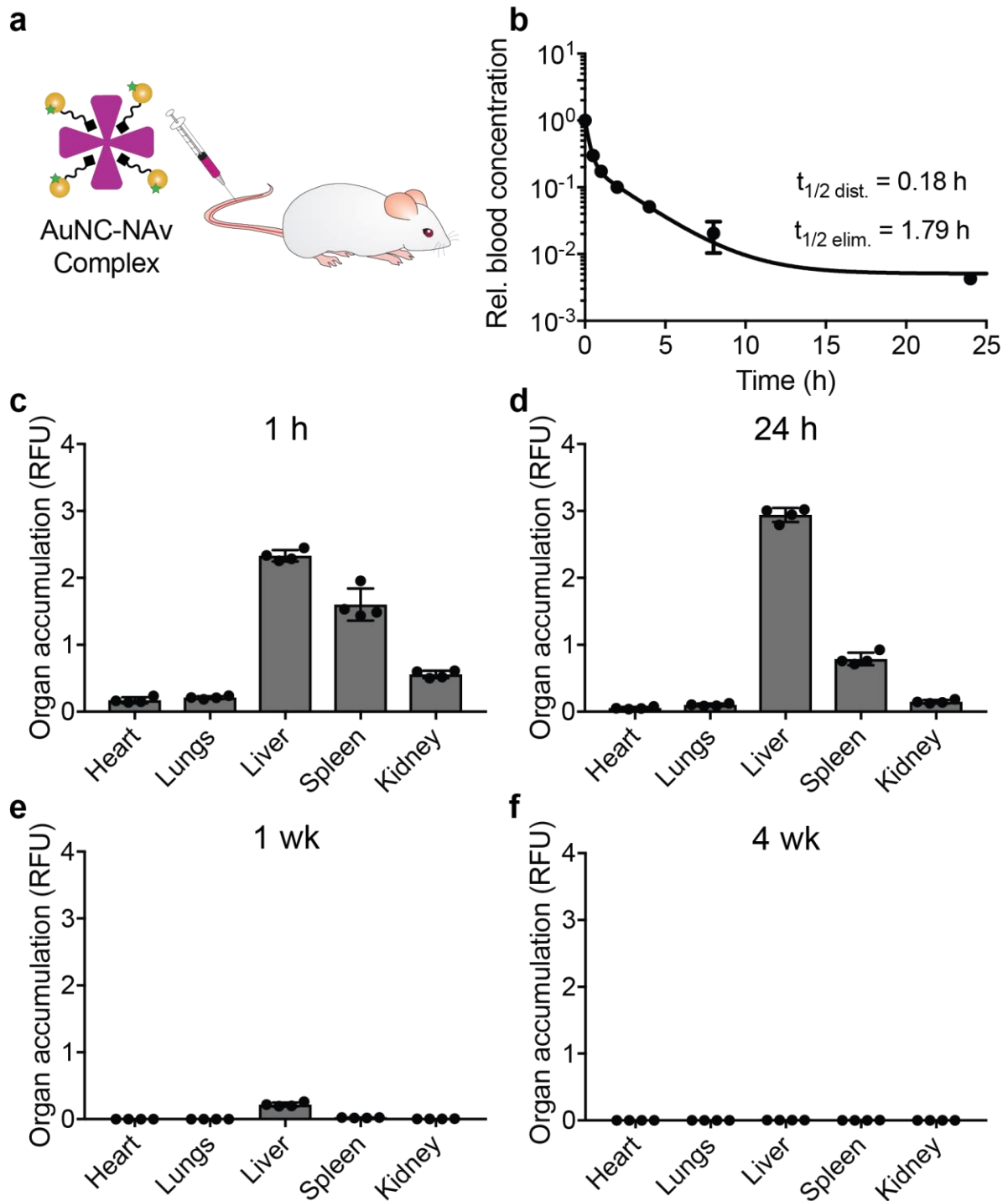




**Supplementary Figure 16.** Biocompatibility of AuNC-NAv complex. (a) *In vitro* cytotoxicity of AuNC-NAv complex towards HEK293T cells, determined by the MTS assay (mean  $\pm$  s.d.,  $n = 3$  biologically independent samples). AuNC-P<sub>20</sub>-NAv at the indicated concentrations was incubated with cells for 24 h. (b) Change in body mass of immunocompetent Swiss Webster mice injected with AuNC-P<sub>120</sub>-NAv (dose = 3000 pmol, 200  $\mu$ L of 15  $\mu$ M [AuNC]) compared with PBS control (mean  $\pm$  s.d.,  $n = 4$  mice per group). There was no statistically significant difference in the mass change over a period of 4 weeks between control mice (PBS injection) and mice injected with AuNC-NAv complex (multiple  $t$ -tests with Holm-Sidak correction for multiple comparisons;  $^{ns}P = 0.936$  for 0, 11, 21, and 28 d;  $^{ns}P = 0.887$  for 5 d). (c) Immunocompetent Swiss Webster mice were i.v. injected with AuNC-P<sub>20</sub>-NAv (dose = 3000 pmol, 200  $\mu$ L of 15  $\mu$ M [AuNC]) and organs (heart, lung, liver, spleen, and kidney) were collected at 1 h, 24 h, and 10 days post administration. Organs were fixed, embedded in paraffin, and stained with hematoxylin & eosin. Analysis by a veterinary pathologist confirmed that tissues from AuNC-NAv injected animals appeared similar to PBS injected controls, exhibiting no signs of toxicity. Study was done with  $n = 3$  mice per group and images from representative animals are shown. Scale bar represents 200  $\mu$ m.

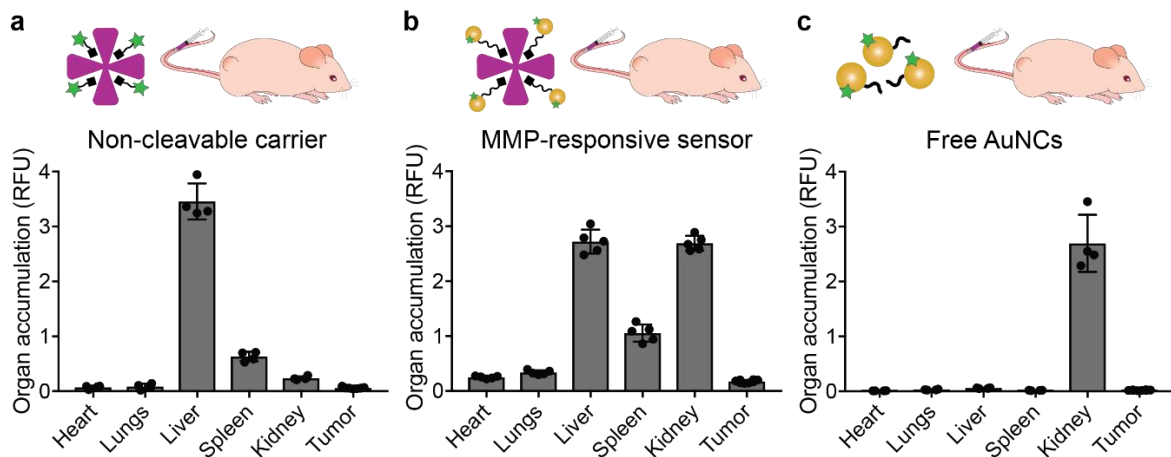


**Supplementary Figure 17.** Organ biodistribution and renal clearance of AuNCs in healthy mice. (a) Schematic of biodistribution and renal clearance study. Near-IR dye labelled GSH-AuNCs were i.v. injected into mice (10  $\mu$ M, 200  $\mu$ L), and urine samples were collected, and major organs harvested at time points up to 7 days p.i. (b) Either IR labelled GSH-AuNCs (GSH-AuNC-IR) or unlabelled GSH-AuNCs were i.v. injected into Swiss Webster mice, and urine was collected 1 h post-injection. Urine was analysed by both TMB catalytic activity assay and by ICP-MS to measure gold content, where both techniques corroborated ca. 47% AuNC clearance compared to the injected dose at 1 h (mean  $\pm$  s.d.,  $n = 4$  mice). (c-f) Organs were harvested at (c) 1 h, (d) 3 h, (e) 24 h, and (f) 1 week after i.v. injection (10  $\mu$ M, 200  $\mu$ L) of near IR-dye labelled GSH-AuNCs into Swiss Webster mice, and the signal intensity in each organ was measured by an Odyssey IR scanner (mean  $\pm$  s.d.,  $n = 4$  mice). Organ accumulation (y-axis) is presented as signal intensity per unit area, calculated for each organ as the difference between the experimental group (near IR-dye labelled GSH-AuNCs) versus the PBS-injected control. GSH-AuNCs accumulated significantly in kidneys 1 h post i.v. administration (one-way ANOVA with Tukey's multiple comparison test, \*\*\*\* $P < 0.0001$ ). Kidney accumulation was significantly reduced 1 week post administration of GSH-AuNCs, likely due to excretion of AuNCs into urine. (g) Renal clearance time course of IR labelled GSH-AuNC or unlabelled GSH-AuNC in collected urine as measured by ICP-MS (estimated ppb cleared), normalized to gold content of the injected dose (mean  $\pm$  s.d.,  $n = 4$  mice). Gold content was below the limit of detection in urine after 24 h p.i., where the detection cut-off was calculated as 3 standard deviations above the mean gold signal from PBS injected control mice (cut-off = 0.13% ID). (h) Kidney accumulation from biodistribution time course monitored up to 1 week p.i. (normalized to 1 h). AuNC signal was undetectable in kidneys at 1 week p.i. (mean  $\pm$  s.d.,  $n = 4$  mice).

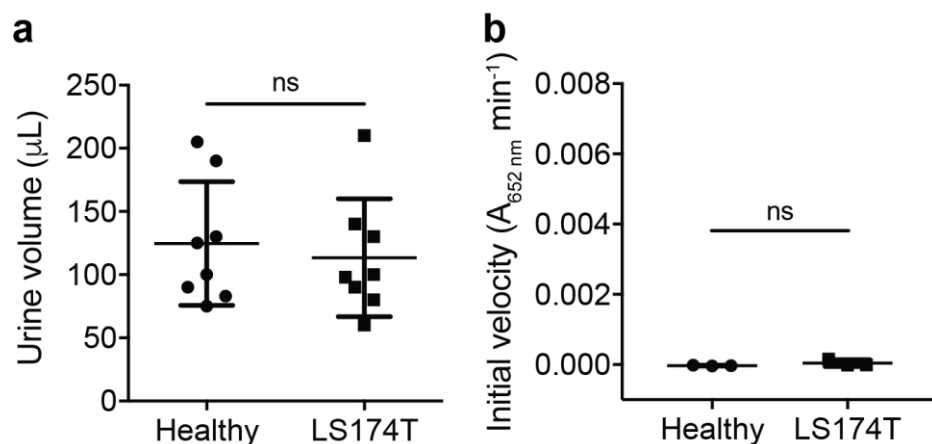


**Supplementary Figure 18.** Time course biodistribution of AuNC-NAv complex in healthy mice. (a) Schematic of biodistribution and pharmacokinetics study, where IR-dye labelled AuNC-P2<sub>20</sub>-NAv complexes were i.v. injected into Swiss Webster mice (15  $\mu$ M, 200  $\mu$ L), and blood samples were collected, and major organs harvested at time points up to 4 weeks p.i. (b) Pharmacokinetic characterization of IR-dye labelled AuNC-P2<sub>20</sub>-NAv complex in Swiss Webster mice. Plasma concentration of nanosensor was fit to a two-phase exponential decay (mean  $\pm$  s.d.,  $n = 5$  mice). Organs were harvested at (c) 1 h, (d) 24 h, (e) 1 week, and (f) 4 weeks after i.v. injection (15  $\mu$ M, 200  $\mu$ L) of near IR-dye labelled AuNC-P2<sub>20</sub>-NAv complex into healthy Swiss Webster mice, and the signal intensity in each organ was measured by an Odyssey IR scanner (mean  $\pm$  s.d.,  $n = 4$  mice). Organ accumulation (y-axis) is presented as signal intensity per unit area, calculated for each organ as the difference between the

experimental group (fluorescently labelled AuNC-NAv complex) versus the PBS-injected control. AuNC signal was maximum at 1 h for all organs except for the liver and was undetectable in all organs at 4 weeks p.i.



**Supplementary Figure 19.** Entry of AuNC nanosensor complexes into tumours at 1 h p.i. Organs and tumours were harvested 1 h after i.v. injection of (a) near IR-dye labelled neutravidin carrier, (b) MMP-cleavable AuNC-P2<sub>20</sub>-NAv complex, where signal arises from contribution of both liberated AuNCs and intact AuNC-NAv complex, or (c) free AuNCs, into LS174T tumour-bearing mice, and the signal intensity in each organ was measured by an Odyssey IR scanner (mean  $\pm$  s.d., (a), (c)  $n = 4$  mice; (b)  $n = 5$  mice). Organ accumulation (y-axis) is presented as signal intensity per unit area, calculated for each organ as the difference between the experimental group (fluorescently labelled carrier, complex, or nanocluster) versus the PBS-injected control.



**Supplementary Figure 20.** Verification of colorimetric disease detection in LS174T tumour model. (a) Collected urine volumes for samples used in colorimetric disease detection experiment (Fig. 5, samples represented in black and dark blue). No statistically significant difference in urine volume was observed between the two groups (mean  $\pm$  s.d.,  $n = 8$  mice per group, two-tailed Student's  $t$ -test,  $^{ns}P = 0.645$ ). (b) Catalytic activity assay on urine from healthy and tumour-bearing mice injected with PBS. No colorimetric development was observed in either group, and there was no statistically significant difference between the two groups (mean  $\pm$  s.d.,  $n = 3$  mice per group, two-tailed Student's  $t$ -test,  $^{ns}P = 0.284$ ).

**Supplementary Table 1.** Sequences of all peptides employed in study. Lowercase indicates d-stereoisomer. Q indicates a quenched substrate with the FAM-CPQ2 FRET pair, where 5FAM is the fluorophore and CPQ2 is the quencher.

<b>Substrate (P<sub>#aa</sub>)</b>	<b>Protease specificity</b>	<b>Sequence (↓ represents scissile bond, enzyme recognition motif bolded.)</b>
P1Q	Thrombin	(5FAM)-GG <b>fPR</b> ↓SGGGK(CPQ2)-(PEG2)-C
P1 <sub>13</sub>	Thrombin	Biotin-SGG <b>fPR</b> ↓SGGSGGC
P1 <sub>20</sub>	Thrombin	Biotin-GGGSGGGSGG <b>fPR</b> ↓SGGGGGC
P2Q	MMP9	(5FAM)-GG <b>PLG</b> ↓VRGKK(CPQ2)-(PEG2)-C
P2 <sub>13</sub>	MMP9	Biotin-GGG <b>PLG</b> ↓VRGKGGC
P2 <sub>20</sub>	MMP9	Biotin-GGGGGGGGG <b>PLG</b> ↓VRGKGGC



**Supplementary Table 2.** Comparison of the kinetic parameters of catalysts toward the oxidation of TMB by H<sub>2</sub>O<sub>2</sub>.

Catalyst	[E] / M	Substrate	K <sub>m</sub> / M	V <sub>max</sub> / M s <sup>-1</sup>	K <sub>cat</sub> / s <sup>-1</sup>
AuNC ca. 1.5 nm	1.8 × 10 <sup>-6</sup>	TMB	2.3 × 10 <sup>-4</sup>	3.6 × 10 <sup>-7</sup>	0.20
HRP <sup>3</sup>	2.5 × 10 <sup>-11</sup>	TMB	4.3 × 10 <sup>-4</sup>	1.0 × 10 <sup>-7</sup>	4.0 × 10 <sup>3</sup>

[E] represents the catalyst concentration, K<sub>m</sub> is the Michaelis constant, V<sub>max</sub> is the maximal reaction velocity, and K<sub>cat</sub> is the catalytic constant that equals V<sub>max</sub>/[E].

Steady-state kinetic assays were carried out at room temperature in a 96-well plate with 220 μL solution with estimated path length (*l*) of 0.5 cm. 25 mM NaOAc/HOAc solution (pH 4.0) was used as the reaction buffer. For kinetic assays varying TMB concentration, AuNCs (20 μM, 20 μL) were mixed with TMB (10 μM to 1 mM, 100 μL) and H<sub>2</sub>O<sub>2</sub> (5 M, 100 μL). The initial reaction velocity (*v*) was calculated by Slope<sub>Initial</sub>/(ε<sub>TMB-652 nm</sub> × *l*), where ε<sub>TMB-652 nm</sub> is the molar extinction coefficient of TMB at 652 nm, which is 3.9 × 10<sup>4</sup> M<sup>-1</sup>·cm<sup>-1</sup>. The plots of reaction velocity, *v*, against TMB concentrations were fitted using nonlinear regression of the Michaelis-Menten equation. The kinetic parameters were calculated based on the Michaelis-Menten equation:  $v = V_{max} \times [S]/(K_m + [S])$ , where V<sub>max</sub> represents the maximal reaction velocity, [S] is the concentration of substrate, and K<sub>m</sub> is the Michaelis constant. V<sub>max</sub> was obtained from fitting to the model using GraphPad Prism software.

**Supplementary Table 3.** Quantification of AuNC cleavage products from *in vitro* gel filtration chromatography assays.

<b>AuNC-NAv complex</b>	<b>% Cleavage (free AuNC fraction: 7 – 12 mL)</b>	<b>Figure reference</b>
AuNC-P1 <sub>13</sub> -NAv + THR (12 h)	21.8%	Fig S13c
AuNC-P1 <sub>20</sub> -NAv + THR (12 h)	90.2%	Fig 4e
AuNC-P1 <sub>20</sub> -NAv + MMP9 (12 h)	7.1%	
AuNC-P2 <sub>13</sub> -NAv + MMP9 (12 h)	15.2%	Fig S13d
AuNC-P2 <sub>20</sub> -NAv + MMP9 (12 h)	75.1%	Fig 4f
AuNC-P2 <sub>20</sub> -NAv + THR (12 h)	5.5%	
AuNC-P2 <sub>20</sub> -NAv + MMP7/9/13 (12 h)	MMP7: 12.1% MMP9: 54.9% MMP13: 29.8%	Fig S13e
AuNC-1:20-P1 <sub>20</sub> -NAv + THR (1 h)	89.9%	Fig S13f
AuNC-1:5-P1 <sub>20</sub> -NAv + THR (1 h)	49.6%	

**Supplementary Table 4.** Gold content analysis in urine as measured by ICP-MS. Urine samples were collected at varying time points from mice injected with either GSH-AuNC-IR or unlabelled GSH-AuNCs (mean  $\pm$  s.d.,  $n = 4$  mice per group), where comparable renal clearance efficiencies were observed between bare and IR dye-labelled AuNCs. Gold signal was undetectable in urine after 24 h p.i., where limit of detection was calculated as 3 standard deviations above the mean gold signal from PBS injected control mice (cut-off = 0.13% ID).

<b>Time (h)</b>	<b>GSH-AuNC-IR (% ID by ICP-MS)</b>	<b>GSH-AuNC (% ID by ICP-MS)</b>
<b>0 – 1</b>	45.13 $\pm$ 7.46	48.20 $\pm$ 9.23
<b>2 – 3</b>	0.89 $\pm$ 0.43	0.87 $\pm$ 0.36
<b>7 – 8</b>	0.57 $\pm$ 0.30	0.52 $\pm$ 0.13
<b>23 – 24</b>	0.19 $\pm$ 0.05	0.23 $\pm$ 0.15
<b>47 – 48</b>	0.13 $\pm$ 0.03	0.13 $\pm$ 0.08
<b>167 – 168</b>	0.07 $\pm$ 0.01	0.02 $\pm$ 0.01
<b>407 – 408</b>	--	0.02 $\pm$ 0.01

## **References:**

1. Kapusta, P. Absolute diffusion coefficients: Compilation of reference data for FCS calibration. *PicoQuant GmbH Appl. Note* (2010).
2. Müller, P., Schwille, P. & Weidemann, T. PyCorrFit-generic data evaluation for fluorescence correlation spectroscopy. *Bioinformatics* **30**, 2532–2533 (2014).
3. Gao, L. *et al.* Intrinsic peroxidase-like activity of ferromagnetic nanoparticles. *Nat. Nanotechnol.* **2**, 577–83 (2007).